430: The effect of preferential view direction on measured surface temperature

C. Adderley[1*], A. Christen[1], F. Meier[2], J. A. Voogt[3]
Department of Geography, University of British Columbia, Vancouver, Canada [1]*
cadderley@gmail.com
Department of Ecology, Technische Universität Berlin, Berlin, Germany [2]
Department of Geography, University of Western Ontario, London, Canada [3]

Abstract

The complete surface temperature $T_{0,C}$ of a complex urban surface is an important parameter in the urban energy balance. As direct measurements of $T_{0,C}$ in an urban setting are difficult, remote sensing techniques are often used to retrieve integrated temperatures, however, these sensors inherently define a preferential view direction and field of view. The goal of this paper is to quantify typical differences between observed temperature $T_{0,p}$ and $T_{0,C}$ for different view geometries over the course of a clear-sky day. A full diurnal course of thermal panoramas were collected using a thermal scanner mounted on a hydraulic tower in a relatively uniform suburban residential area in Vancouver, Canada. The panoramas are combined with a high-detail 3D model of the urban form constructed via photogrammetry. Computer vision techniques are used to match thermal pixels to their world locations and attribute material, slope, aspect, sky view factor and relative altitude to them. Corrections are applied for atmospheric transmission and surface emissivity effects. Computer graphics techniques are then used to simulate the view of a sensor placed at varying azimuths and off-nadir angles. The complete surface temperature $T_{0,C}$ was then computed and compared to the simulated sensor view temperature It was found that during the daytime situation, simulated sensor temperature $T_{0,p}$ was higher than $T_{0,C}$, by up to 3.8 K, while in the night-time situation the reverse was true, by up to -2.84 K. A significant anisotropy was observed during the daytime (up to 4.3 K) which caused variation in the difference between $T_{0,C}$ and $T_{0,p}$ when sensor azimuth and off-nadir angle changes.

Keywords: Urban surface temperature, complete surface temperatures, thermal anisotropy, multiple view directions

1. Introduction

The complete surface temperature $T_{0,C}$ [1] of a complex urban surface is a key parameter in the urban energy balance. A direct measurement of $T_{0,C}$ in an urban setting, however, is difficult. The surface temperature of individual facets $T_{0,f}$ varies considerably due to shading and view factor heterogeneity [2]. Most commonly, remote sensing techniques are applied to recover integrated surface temperatures, but these techniques inherently define a preferential view direction and field of view (e.g. hemispheric, plan view, oblique view) in which the observed temperature $T_{0,p}$ is not necessarily equal to $T_{0,C}$. The goal of this project is to quantify typical differences between the surface temperature sensed by the preferential view direction of typical systems $T_{0,p}$ and the complete surface temperature $T_{0,C}$ for a typical urban surface over the course of a clear-sky day. Thermal anisotropy is expected to be maximized under clear-sky conditions [2].

2. Study Area

The case study was performed at the 6100 block of Elgin Street in Vancouver, Canada. This street is characterized by a relatively uniform suburban residential form consisting of two-story residential houses (h = 6.5 m) with similar materials and morphometry ,located along a 60 m canyon with a wide street (9.5 m), large front lawns and an absence of tall trees.

3. Experimental Setup

On September 14 and 15th 2008 a Thermovision A40M thermal scanner was emplaced on a 15 m hydraulic tower in the centre of the target street canyon (at coordinates 49.2283° N, 123.0838° W). The placement is shown in Fig 1.

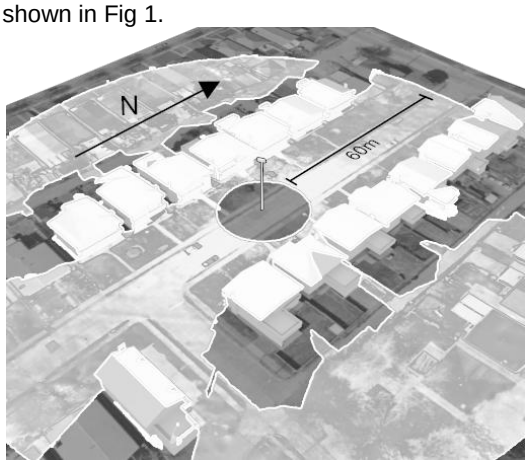

Fig 1. Elgin Street canyon with location of scanner in centre. Areas visible in panoramas are shown highlighted, dark areas are obscured

The scanner has a spectral response from 7 to 15 µm and was equipped with a 45° field of view lens. The camera was operated remotely with a pan and tilt device. From 13:30 PST on September 14th to 15:30 PST on September 15th panoramic sweeps of the canyon were performed. Two panoramas were taken every 30 minutes, one at an angle 68° from nadir and another at 45° from nadir. Each panorama covered the full 360° of the canyon, providing high detail coverage at close range, with low detail coverage useful up to 60 metres from the scanner (coverage shown in Fig 1). Pixel instantaneous field of view ranged from 3 cm/px to 1 m/px).

This produced a full diurnal course of panoramic thermal images of the study area (example in Fig 2), containing a representative sample of surfaces of all orientations (azimuth and elevation) and material properties.

Fig 2. Example of stitched panorama created from thermal images taken at 12:00 PST (south facing at top, north facing below). White represents warmer surfaces.

A highly detailed 3D model of the urban canyon was constructed using a combination of differential GPS survey points, airborne LiDaR surface data (5-15 returns per m^2), orthorectified aerial photography, and close-range ground-based photogrammetry. This model incorporated both geometric and surface information, ranging from inherent parameters, such as material and facet type, to derived properties, such as facet emissivity and calculated sky view factor.

4. Data Processing

4.1 Atmospheric and Emissivity Corrections

The thermal panoramas were then combined with the 3D model via computer vision techniques. Pixels on the panoramas were matched with their corresponding world locations, associating each pixel in the 3D model with a brightness temperature. Using calculated camera to pixel distances (line of sight) along with the underlying information in the model, two corrections were applied. Firstly, an atmospheric correction was performed using MODTRAN simulations completed (method used by Meier et al. [3]) for the range of meteorological conditions during the measurement campaign.

Secondly, an emissivity correction using surface classification data was performed. Each pixel's sky view factor was used to weigh the proportion of longwave radiation input from sky (measured on a nearby 30 tower, assuming isotropic distribution) and ground (averaged over the entire 3D model). Solving the local longwave radiation balance for each pixel using these incoming radiation fluxes and the known outgoing radiation flux (from the pixel radiant temperature and emissivity) allows the calculation of a meaningful value for true surface temperature.

4.2 Gap Filling

Many surfaces were obscured from the thermal scanner due to blocking from other objects in the canyon, and thus had no associated temperature values. Other areas were incorrectly attributed or contained objects that were not part of the 3D model, such as cars. These areas were masked out. However, to calculate $T_{0,C}$, temperatures for these surfaces must be known. It was therefore necessary to develop a gap-filling algorithm that would associate meaningful temperatures to obscured and masked areas. This was implemented via an adaptive search procedure in which four indices (facet type, facet orientation, material and sky view factor) of an obscured pixel were used to locate similar pixels that do have temperature information. Because of the panoramic nature of the data, this meant that a corresponding facet could be found possibly in the opposite view direction. This information was averaged and assigned to these obscured pixels.

5. Results

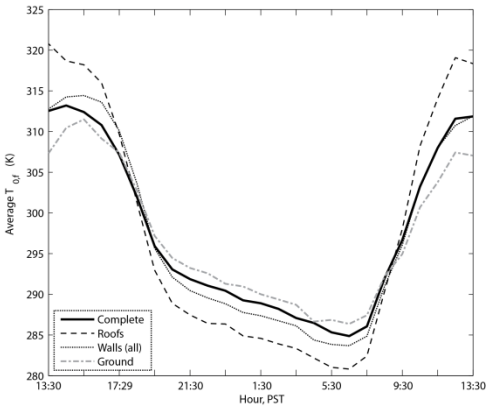

Fig 3. Spatially averaged surface temperatures for the street canyon during the experiment

The resulting database of surface temperatures and associated geometric and material information allowed the complete surface temperature of the canyon to be computed. Fig 3 presents the spatially averaged facet temperature $T_{0,f}$ (each pixel weighted by its area) over the diurnal course of the three major facet types (roof, wall, ground) along with the spatially averaged complete surface temperature of the urban system $T_{0,C}$. We observe expected patterns during the diurnal course, for example roofs being warmer by day and colder at night. Fig 4 displays the wall temperatures split by facet orientation in additional detail. Again, the pattern is as expected for a mid-latitude northern

hemisphere city, with south-facing walls being generally warmer in the daytime, west-facing walls being warmest in the afternoon, and east-facing walls warmest in the morning.

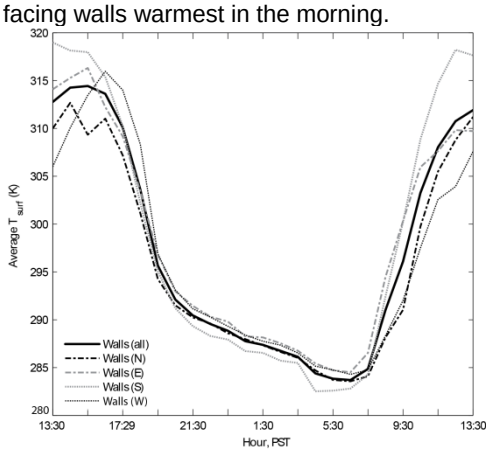

Fig 4. Spatially averaged wall surface temperatures during the experiment, separated by orientation

6. Analysis

The 3D model and associated temperatures were then imported into CAD software to perform preferential view direction simulations. As remote sensors often observe a larger area than a single city block, the model was treated as a repeatable element and duplicated several thousand times in order to create a meaningful surface (effectively infinite to a virtual camera).

Fig 5. Repeated city blocks as viewed by the virtual camera at elevation 50 degrees, azimuth 210 degrees. The repeated element is outlined in black.

To simulate a sensor at an arbitrary nadir angle and orientation, a virtual pinhole camera was positioned at 1000 metres directly above the model surface and the resulting view rendered. The camera was then positioned at off-nadir angles (from 10 to 70° at 10 degree increments) and varying azimuths (from 0 to 360° at 20° increments) and rendered. An example sensor view is shown in Fig 5. This produced a set of simulated sensor images which were averaged (each pixel equally weighted) to find the value of $T_{0,p}$ for each combination of off-nadir angle and azimuth. The difference between $T_{0,p}$ and $T_{0,C}$ can then be quantified. Polar plots showing this difference for several time steps are shown in Fig 6.

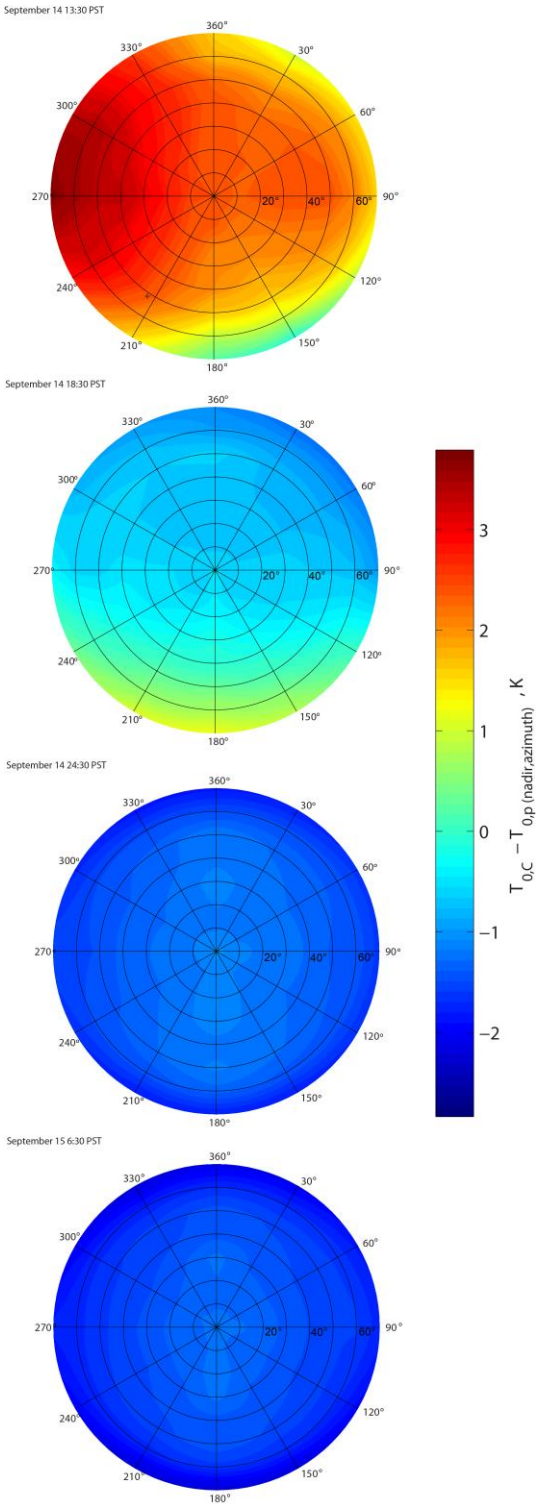

Fig 6. Computed difference between $T_{0,C}$ and $T_{0,p}$ for a planar sensor at various time step.s Color axis remains the same in all plots. Centre of the plot has the sensor at nadir, moving away from the centre increases the off-nadir angle for a given azimuth.

These plots show that the complete surface temperature represents the sensor view

only at certain times and certain view directions. In the daytime situation, $T_{0,C}$ is often lower than $T_{0,p}$, while in the night-time situation this is reversed. The effects of thermal anisotropy are also present and important, creating large variations in temperature across the plot at this reasonably small scale. The anisotropy performs as expected, being maximized in the morning and the afternoon, with lower values in the evening and being almost nonexistent late at night.

7. Conclusions

A novel methodology was developed to quantify the complete surface temperature and simulate preferential view directions. A single thermal scanner with a panoramic sweep in an urban area of uniform structure collected a large sample of temperatures from facets with different orientations and materials. Images were projected on the surface of a 3D model, and unseen facets were statistically filled using similar facets from other parts of the panorama. This methodology allowed the reconstruction of a block scale model of brightness temperature as a function of time over 24 hours.

Simulated plan view temperatures show differences of +3.8 K to -2.84 K from the calculated complete surface temperature. Generally $T_{0,C}$ is higher in the night-time situation and lower in the daytime situation due to facets that are invisible to the simulated sensor. Warmer wall surfaces at night will cause $T_{0,C}$ to be higher, while at the same time cooler roofs and ground surfaces make up much of the field of view of the sensor, reducing $T_{0,p}$. Similar effects cause $T_{0,p}$ to be higher in the daytime (warmer roofs, less view of cooler wall) and $T_{0,C}$ to be lower (taking the cool walls into account).

This difference can be quantified by the thermal anisotropy (difference between maximum and minimum observed $T_{0,p}$ at a single time step). This measure was lowest at night (0.74 K at 5:30 PST), and highest in the morning and afternoon (up to 4.3 K at 7:30 PST). Overall over the entire time series, the RMS error between $T_{0,C}$ and $T_{0,p}$ was 0.7 K, which shows good agreement but does not represent the large anisotropy observed when viewing angles deviate from nadir.

8. Acknowledgements

This study was supported by the Canadian Foundation for Climate and Atmospheric Sciences (CFCAS) as part of the Network Grant 'Environmental Prediction in Canadian Cities' (EPiCC), by NSERC Discovery Grants (Christen, Voogt). Selected equipment was provided by Environment Canada and M. Church, UBC Geography. We thank Brett Eaton (UBC Geography), Bob Woodham (UBC Computer Science), Frederic Chagnon (Environment Canada), Ben Crawford (UBC), Adrian Jones (UBC), Rick Ketler (UBC), Ivan Liu (UBC), Kate Liss (UBC), Tim Oke (UBC), Chad Siemens (UBC), and Derek van der Kamp (UBC).

9. References

1. Voogt, J. A., and Oke, T. R. (1997). Complete urban surface temperatures. *Journal of Applied Meteorology*, 36: p.1117–1132.

2. Voogt, J. A., and Oke, T.R. (1998). Effects of urban surface geometry on remotely-sensed surface temperature. International Journal of Remote Sensing, 19: p. 895-920.

3. Meier, F., Scherer, D., Richters, J., Christen, A. (2011). Atmospheric correction of thermal-infrared imagery of the 3-D urban environment acquired in oblique viewing geometry. *Atmospheric Measurement Techniques*, 4: p. 909-922.